Journal of the Electrochemical Society

The Electrochemical Society
Advancing solid state & electrochemical science & technology

Evaluating the High-Voltage Stability of Conductive Carbon and Ethylene Carbonate with Various Lithium Salts

Journal of The Electrochemical Society, 2020 **167** 160522

Evaluating the High-Voltage Stability of Conductive Carbon and Ethylene Carbonate with Various Lithium Salts

Michael Metzger,[1,*] Patrick Walke,[1] Sophie Solchenbach,[1,z] Gregory Salitra,[2,*] Doron Aurbach,[2,] and Hubert A. Gasteiger[1,**]**

[1]*Chair of Technical Electrochemistry, Department of Chemistry and Catalysis Research Center, Technische Universität München, D-85748 Garching, Germany*
[2]*Department of Chemistry and BINA (BIU center of nano-technology and advanced materials), Bar-Ilan University, Ramat-Gan 52900, Israel*

The anodic stability of conductive carbon and alkyl carbonate-based electrolyte solvents is a crucial requirement for the success of high-voltage lithium-ion cells, particularly at elevated temperatures. In order to quantify the oxidative stability of ethylene carbonate (EC), a critical component of lithium-ion battery electrolytes, and conductive carbons, we have evaluated the stability of a ^{13}C-labeled conductive carbon and an EC-based electrolyte up to 5.5 V vs Li^+/Li. We examined the behavior between 25 °C and 60 °C for four different lithium salts ($LiClO_4$, $LiPF_6$, LiTFSI, and $LiBF_4$). This is done by means of On-line Electrochemical Mass Spectrometry (OEMS), whereby the isotopically labeled carbon is used to differentiate between the CO and CO_2 evolution from the oxidation of the conductive carbon ($^{13}CO/^{13}CO_2$) and of the electrolyte ($^{12}CO/^{12}CO_2$). Our analysis reveals that conductive carbon is stable with $LiPF_6$, however, pronounced electrolyte oxidation and gaseous byproducts like HF, PF_5 and POF_3 are observed. $LiBF_4$ provides an excellent carbon and electrolyte stability even at 50 °C, rendering it as a better salt than $LiPF_6$ for the cathode side in high-voltage lithium-ion cells.

 [DOI: 10.1149/1945-7111/abcabd]

Manuscript submitted October 6, 2020; revised manuscript received November 11, 2020. Published December 2, 2020.

Supplementary material for this article is available online

In the light of recent progress on high-voltage cathode materials for lithium-ion batteries the choice of lithium salt for battery electrolytes should be revisited. Lithium hexafluorophosphate ($LiPF_6$) has been the main lithium salt in rechargeable lithium-ion batteries for more than 25 years.[1] Compared to other lithium salts, $LiPF_6$ provides among the highest conductivities for Li^+-ions when dissolved at 1–2 M in alky carbonate solutions.[2,3] The alkyl carbonate based solutions are typically ethylene carbonate (EC) mixed with ethylmethylcarbonate (EMC), diethlycarbonate (DEC) or dimethylcarbonate (DMC); more recently, EC-free electrolytes have been proposed, which in the majority also utilize $LiPF_6$ as the main lithium salt.[4–6] Furthermore, LiF and other fluorine species derived from $LiPF_6$ in the passivation process of the graphite negative electrodes seem to contribute to the formation of stable surface films that behave like a very good protecting solid-electrolyte interphase (SEI).[7,8] Alkyl carbonate solutions containing $LiPF_6$ were also shown to passivate aluminum during anodic polarization through surface films containing AlF_3, Al_2O_3, and $Al(OH)_3$,[9,10] an important prerequisite for the use of aluminum as current collector on the cathode side of lithium-ion batteries. The anodic stability of $LiPF_6$-based electrolyte is typically considered sufficient to cycle lithium-ion batteries within a restricted voltage window and at moderate temperatures, but strong capacity fading sets in at high cathode potentials (>4.5 V vs Li^+/Li for an NMC111 cathode at 25 °C)[11] and at high temperature (around 60 °C for NMC111 cycled to 4.3 V vs Li^+/Li).[12] At elevated temperature, e.g., upon storage at 85 °C, $LiPF_6$ can decompose into LiF and PF_5,[13,14] depleting the electrolyte solution of free Li^+-ions and eventually decreasing its conductivity. PF_5 is a highly reactive Lewis acid, which can decompose organic carbonate solvent molecules and the organic SEI into gaseous products.[13–15]

When using $LiPF_6$ in high-voltage lithium-ion batteries (>4.5 V vs Li^+/Li) the following problems arise: (i) There is a larger gas generation in cells with $LiPF_6$ than in cells containing other lithium salts, e.g., lithium tetrafluoroborate ($LiBF_4$).[16] (ii) The salt reacts with H_2O to POF_3,[11,17,18] or other protic species[19] formed by the chemical or electrochemical oxidation of organic electrolyte.[20] (iii) The latter side reactions form HF, which in turn can dissolve transition metals from the positive electrode.[12,21,22] Thus, more transition metal dissolution is found in cells with $LiPF_6$ operated at high voltage than, e.g., in cells with $LiBF_4$.[21] (iv) The detection of gases derived from $LiPF_6$ (e.g., PF_5 or POF_3) indicates that the processes at high voltage also lead to a decomposition of the salt, much like the processes at high temperature.[14,17,23–25] All in all, this puts in question the viability of $LiPF_6$ as lithium salt for high-voltage lithium ion cells and necessitates alternative lithium salts that provide higher stability at the operating voltages of next generation cathode materials.

In our previous work, we developed a method to study the electrooxidation of alkyl carbonate-based electrolyte and conductive carbon, in which the type and quantity of generated gases serve as a figure-of-merit to quantify the reactivity of lithium ion salts.[26] We used isotopically labeled ethylene carbonate ($^{13}C_3$-labeled EC) to differentiate between the decomposition of conductive carbon and electrolyte, as well as a two-compartment cell to suppress effects from the counter-electrode and to suppress crosstalk phenomena[27] by separating the anode and cathode compartments by an impermeable lithium ion conducting solid electrolyte. By quantifying the concentration of CO_2 and CO, we could derive anodic oxidation rates for both the conductive carbon and the electrolyte solvent. Using these rates, we extrapolated the weight loss expected to occur in lithium-ion cells when charging to voltages around 5 V vs Li^+/Li. In particular, the work aimed at understanding the effect of temperature and water contamination on the anodic oxidation rates, so we had to choose a lithium salt that is stable at elevated temperature and does not cause side reactions with trace water. Thus, we selected lithium perchlorate ($LiClO_4$). With this salt, substantial carbon oxidation (>7 wt.% carbon loss over 100 h) was found at 5.0 V vs Li^+/Li for temperatures >40 °C.[26] Based on these data with $LiClO_4$ salt, we concluded that the oxidation of conductive carbons can play a role as a potential aging mechanism in high-voltage cells.

Dahn's group investigated impedance growth in high-voltage NMC442/graphite cells using a transmission line model.[28] It was found that the impact of an electronic resistance in the electrode

*Electrochemical Society Active Member.
**Electrochemical Society Fellow.
[z]E-mail: sophie.solchenbach@tum.de

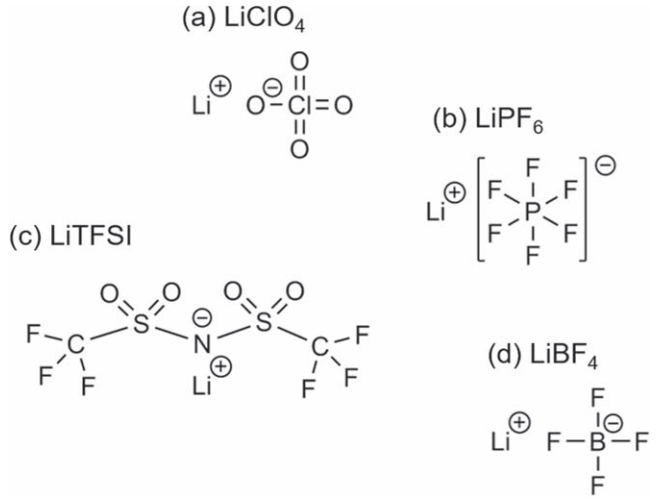

Figure 1. Structure of the conducting salts $LiClO_4$ (lithium perchlorate), $LiPF_6$ (lithium hexafluorophosphate), LiTFSI (lithium bistrifluoromethanesulfonimidate), and $LiBF_4$ (lithium tetrafluoroborate) used in this work.

from oxidation of the conducting carbon network on the overall impedance growth was lower than we had estimated. The lithium salt in this study by Abarbanel et al. was $LiPF_6$ and the maximum cathode voltage was ~4.6 V vs Li^+/Li.[28] Consequently, either the lower voltage or the choice of lithium salt led to a much lower impact of carbon oxidation than suggested by our measurements with $LiClO_4$. Similarly, while cycling an LNMO ($LiNi_{0.5}Mn_{1.5}O_4$) cathode with an $LiPF_6$-based electrolyte in a graphite/LNMO cell to an upper cutoff voltage of 4.8 V (~4.9 V vs Li^+/Li) at 40 °C resulted in an increasingly pronounced contact resistance at the cathode/current collector interface, it could be clearly ascribed to the formation of an insulating surface film on the aluminum current collector rather than to the corrosion of the conductive carbon.[29] These observations suggest that the corrosion of conductive carbons is much less significant with $LiPF_6$ compared to $LiClO_4$ salt, calling for additional measurements to quantify this difference.

Another interesting lithium salt to examine in this context is $LiBF_4$, which had recently been revisited by Dahn's group as a candidate salt for high-voltage cells.[30] In a comparative study, the use of $LiBF_4$ showed a benefit over $LiPF_6$ in terms of a low charge transfer resistance at the positive electrode when cycling up to 4.5 V vs Li^+/Li. However, it still showed an impedance growth due to an increased charge transfer resistance at the negative electrode, indicating poor passivation of the negative electrode.[30] Dahn's group also investigated synergistic effects of combining $LiPF_6$ and $LiBF_4$.[16] It was found that electrolytes consisting of equal amounts of $LiBF_4$ and $LiPF_6$ show better performance in high-voltage lithium-ion cells charged to 4.45 V vs Li^+/Li than electrolytes with $LiPF_6$ or $LiBF_4$ alone. Again, this was attributed to the reduced impedance growth at the positive electrode with $LiBF_4$, while $LiPF_6$ was thought to improve the passivation at the negative electrode. Finally, Shen et al. discovered that $LiBF_4$ outperforms $LiPF_6$ in terms of capacity retention in positive/positive symmetric cells.[31] With this technique, only reactions at the cathode are evaluated, further suggesting that $LiBF_4$ works well at high voltage. All in all, these articles suggest that $LiBF_4$ is a promising conductive salt for high-voltage lithium-ion cells.

In light of these new findings, we wanted to extend our previous analysis with $LiClO_4$ and examine in the present study the oxidative stability of conductive carbon and the electrolyte solution with other more application-relevant lithium salts, viz., $LiPF_6$, $LiBF_4$, and lithium bistrifluoromethanesulfonimidate (LiTFSI). Specifically, we have quantified the effect of these four salts (see Fig. 1) on the electro-oxidation of conductive carbon and of electrolyte solution using 1.5 M of the respective salt and EC solvent as a main component, hence "EC-only" electrolyte. Once more, we have used isotope labelling to de-convolute the contribution of carbon and electrolyte solution oxidation to CO_2 and CO, which evolution in the cells during positive polarization was explored. This time, however, we have chosen a ^{13}C-labeled conductive carbon instead of $^{13}C_3$-labeled EC. For *operando* gas quantification, we used On-line Electrochemical Mass Spectrometry (OEMS) and a sealed two-compartment cells.[19,26,32]

Experimental

^{13}C conductive carbon electrodes and ^{12}C-based EC-only electrolytes.—In the course of this study, we differentiated between carbon and electrolyte solution oxidation by using fully ^{13}C-labeled carbon (BET area of 145 $m^2\ g^{-1}$, 99 atom% ^{13}C, Sigma Aldrich, Germany) as the working-electrode and regular ^{12}C-based ethylene carbonate (furtheron referred to as $^{12}C_3$ EC; BASF, Germany) as the solvent.

The conductive carbon electrodes were fabricated by mixing 67 wt.% ^{13}C-labeled carbon and 33 wt.% polyvinylidene fluoride binder (PVdF, Kynar HSV 900, Arkema, France) in 1-methyl-2-pyrrolidinone (NMP, Sigma-Aldrich, Germany) for 5 min at 2000 rpm and 50 mbar in a planetary orbital mixer (Thinky, USA). The slurry was coated onto a PET separator (Freudenberg, Germany) using a 250 μm gap bar coater (RK PrintCoat Instruments, UK). After drying on a hot plate at 60 °C for at least 12 h, the electrode tapes were punched into electrodes with a diameter of 15 mm (≡1.77 cm^2). All electrodes were further dried at 120 °C for at least 12 h under dynamic vacuum in a glass oven (Büchi, Switzerland) and then transferred into an argon filled glove box (O_2 and H_2O < 0.1 ppm, MBraun, Germany) avoiding any exposure to ambient air. The exact weight of the carbon electrodes was determined by weighing the dried electrodes and subtracting the areal weight of the PET separator, resulting in an average carbon loading of the electrodes of ~1 $mg_C\ cm^{-2}$.

The electrolyte solutions were prepared by mixing the $^{12}C_3$ EC with the conducting salts $LiClO_4$, $LiPF_6$, LiTFSI, or $LiBF_4$ (all from BASF) at a 1.5 M concentration, hence "EC-only" electrolyte. Upon mixing the salt with solid EC, a liquid solution was obtained due to freezing point depression, further on referred to as $^{12}C_3$ EC electrolytes. 1.5 M salt concentration was chosen, since 1.0 M—the common concentration of lithium salts in most battery electrolytes—leads to high viscosity of the EC-only electrolyte and insufficient wetting of most separators. All electrolyte solutions were prepared in polypropylene (PP) vials and vacuum-dried at 70 °C for at least 12 h. The as-prepared electrolyte solution contained <20 ppm water as determined by Karl-Fischer titration (Titroline KF, Schott Instruments, Germany).

On-line electrochemical mass spectrometry (OEMS).—Before cell assembly in the argon filled glove box, our custom-made two-compartment cell hardware,[26] PET separator sheets (diameter 17 mm, Freudenberg, Germany) and glass fiber separator sheets (diameter 24 mm, VWR, Germany) were vacuum-dried for at least 12 h; the cell hardware was dried at 70 °C, the separators at 120 °C. The Freudenberg PET separators were selected for the upper compartment of the two-compartment cell that is connected to the mass spectrometer inlet in order to avoid the use of glass fiber sheets that participate in side reactions with species that are produced at high voltage (e.g., $SiO_2 + 4HF \rightarrow SiF_4 + 2H_2O$).[24] However, due to the instability of the PET separator in contact with metallic lithium and the fact that the commonly used Celgard® separators were not wetted by the $^{12}C_3$ EC electrolyte, a glass fiber separator (glass microfiber filter, 691, VWR, Germany) was used in the lower compartment that is separated from the upper compartment by an impermeable lithium ion conducting electrolyte membrane.

The metallic lithium counter-electrode (diameter 17 mm, Rockwood Lithium, USA) and a glass fiber separator (diameter 28 mm) were placed in the cell and 160 μl of EC-based electrolyte

with the respective conducting salt were added. Subsequently, a Li^+-ion conductive glass ceramic (diameter 1 inch, thickness 150 μm, conductivity 10^{-4} S cm^{-1} at 25 °C, Ohara, Japan) laminated with Al- and PP-foil was placed on top to separate the anode and cathode compartment (see Refs. 13 and 19 for details on lamination and cell assembly). A PET separator sheet (diameter 17 mm) and the ^{13}C carbon working-electrode (diameter 15 mm) were placed in the upper compartment and 240 μl of electrolyte were added. Since the ^{13}C carbon working-electrode is coated on an insulating PET separator, we use a stainless steel mesh (diameter 21 mm, wire diameter 0.22 mm, openings 1.0 mm, Spoerl KG, Germany) placed on top of the working-electrode as current collector and compress the cell stack with a stainless steel spring (2.3 N mm^{-1}, 0.5 inch diameter and length, Lee Springs, UK) that is attached to the OEMS cell body. An illustration can be found in Fig. 1 of our original article.[26] After assembly in the glove box, the OEMS cell was placed into a temperature-controlled chamber (KB 23, Binder, Germany) set to the desired measurement temperature (25 °C, 35 °C, 50 °C or 60 °C). The cell was first flushed for 2 min with pure Ar to avoid contamination with impurities like CO_2 and N_2 from the glove box atmosphere. Then it was held at open-circuit voltage (OCV; ≈3 V vs Li^+/Li) for 2 h to record a baseline for all ion current signals (m/z = 1 to 128). Subsequently, a linear sweep voltammetry (LSV) procedure is applied at a scan rate of 0.1 mV s^{-1} (Series G300 potentiostat, Gamry, USA) from 3.0 to 5.5 V vs Li^+/Li. The gas evolution during this procedure was recorded by OEMS.

Conversion of the mass spectrometer currents to concentrations was done for the $^{12}CO_2$ and $^{13}CO_2$ carbon dioxide isotopes and the ^{12}CO and ^{13}CO carbon monoxide isotopes, using a calibration gas (Ar with 2000 ppm H_2, O_2, CO and CO_2, Westfalen, Germany) and taking into account the well-detectable 1.1% natural abundance of ^{13}C. Due to the limited isotopic purity of the ^{13}C-labeled carbon (isotopic purity 99 atom% ^{13}C, Sigma-Aldrich, Germany), we applied the following corrections when analyzing the mass signals. The $^{12}CO_2$ signal (m/z = 44) which represents the oxidation of electrolyte was obtained by subtracting 1% of the current at m/z = 45 ($^{13}CO_2$ from oxidation of the ^{13}C-labeled carbon electrode) in order to account for the 1% isotopic ^{12}C impurity in the labeled carbon: I_{44} (electrolyte) = $I_{44} - 0.01 \cdot I_{45}$. An analogous correction was applied to obtain the ^{12}CO signal (m/z = 28) derived from electrolyte in addition to subtracting 14% of the measured m/z = 44 signal to account for the CO_2 fragmentation in our mass spectrometer system: I_{28} (electrolyte) = $I_{28} - 0.01 \cdot I_{29} - 0.14 \cdot I_{44}$ (note that for the used electron energy of 70 eV, one would expect roughly 11% fragmentation,[33] but the exact value for our system determined with a 10% CO_2 in Ar calibration gas was 14%, likely due to the fact that the mass spectrometer system was kept at 100 °C rather than at 25 °C).[32] Since the EC solvent is not solely comprised of ^{12}C atoms, but also has 1.1% natural abundance of ^{13}C, we needed to correct the $^{13}CO_2$ and ^{13}CO signals in a similar way as their ^{12}C counterparts. The $^{13}CO_2$ signal (m/z = 45) stemming from carbon oxidation was corrected for 1% of the $^{12}CO_2$ signal to cancel out naturally abundant $^{13}CO_2$ which actually stems from electrolyte oxidation: I_{45} (carbon) = $I_{45} - 0.01 \cdot I_{44}$. Similarly, the ^{13}CO signal (m/z = 29) derived from carbon oxidation is corrected for the 1% natural abundance of ^{13}CO from the electrolyte and 14% mass fragmentation of $^{13}CO_2$: I_{29} (carbon) = $I_{29} - 0.01 \cdot I_{28} - 0.14 \cdot I_{45}$. In our previous work,[26] we assessed the anodic stability of the PVdF binder and could show that it has no significant contribution to the measured gas evolution within 3.0 to 5.5 V vs Li^+/Li (see Fig. 11 in Ref. 26) such that we do not need to correct the $^{12}CO_2$ and ^{12}CO signals for any contributions from PVdF decomposition.

Spectroscopic techniques.—Raman spectra of Super C65 (68 m^2 g^{-1}, Timcal, Switzerland) and the ^{13}C conductive carbon were acquired with a Senterra Raman spectrometer (Bruker Optics, USA) at a wavelength of 488 nm with a data collection time of 20 s per spectrum. The X-ray photoelectron spectroscopy (XPS) data was recorded with a Kratos Axis-HS spectrometer (Kratos, UK) at a residual gas pressure of ∼$5 \cdot 10^{-10}$ Torr using monochromatized Al K_α radiation ($h\nu$ = 1486.7 eV). The grafoil working-electrodes (calendared and exfoliated natural flake graphite, 19 m^2 g^{-1}, GrafTech, USA) used for ex situ XPS measurements were washed with acetone, dried, and reduced under 5% H_2 in Ar at 900 °C for 12 h prior to the measurement, to obtain binder-free, H-terminated, flat electrodes that allowed for a good signal identification of the XPS measurements. The electrodes were polarized vs metallic lithium in a linear potential sweep to 5.5 V vs Li^+/Li at 1 mV s^{-1} and 25 °C using the same cell hardware as for the OEMS experiments, however, without the Ohara glass separation (i.e., in a one-compartment cell configuration). Subsequently, the cell was disassembled in an argon filled glove box and the harvested working-electrode was washed by immersion in ∼1 ml of dimethyl carbonate (DMC) solvent in a clean and dry PP vial. Reference samples were soaked with electrolyte solution in PP vials for the same amount of time that the linear potential sweep took (∼7 h) and then washed in the same way. After washing, the solvent was evaporated at room temperature under dynamic vacuum for at least 12 h, before the samples were cut with a scalpel, and mounted onto the sample holder using UHV-compatible carbon tape. All spectra were corrected with respect to the binding energy value of the graphite C 1s peak at 284.4 eV. The core peaks were analyzed using a Shirley-type background. For transferring the air sensitive samples into the spectrometer, a custom-made transfer vessel was used, which employs a magnetic manipulator and a gate valve.

Results

Degree of graphitization for ^{13}C conductive carbon and super C65.—Raman spectroscopy was employed to assess the degree of graphitization of the ^{13}C carbon in comparison to Super C65, a typical conductive carbon used in lithium-ion battery cathodes. The degree of graphitization is an important parameter for this study, since highly graphitized carbons usually possess greater anodic stability,[34] due to their higher ratio of basal sites to edge sites.[35] In the supercapacitor literature, the anodic stability of different carbon types has been studied extensively.[35] Single walled carbon nanotubes and mesoporous graphene have been found to exhibit excellent high voltage stability since they possess a high ratio of basal to edge sites, as opposed to amorphous carbon.[36] In Raman spectra of carbonaceous samples the G-band is associated with ideal sp^2-hybridized carbon systems (fully graphitized, e.g., graphene), while the D-band indicates the presence of disorder or sp^3 hybridization. Figure 2 shows that the integral D- to G-band ratio of ^{13}C carbon (D/G = 1.15) is very close to the one of Super C65 (D/G = 1.18). Thus, the two carbons possess a similar degree of graphitization, which implies that the anodic stability of the employed ^{13}C carbon is comparable to typical conductive carbons used in lithium-ion battery cathodes. Moreover, the Raman spectrum reveals the expected isotope downshift of 3.9% for ^{13}C carbon resulting from the heavier ^{13}C atoms.[17]

CO_2 and CO evolution from anodic oxidation with different lithium salts.—Figure 3 summarizes the results of the linear potential sweeps with ^{13}C carbon working-electrodes vs metallic lithium in 1.5 M $LiClO_4$ $^{12}C_3$ EC electrolyte at 25 °C, 35 °C and 50 °C. Each temperature represents an individual measurement. The upper panel (a) of Fig. 3 shows the current-potential curves for the potential sweep from 3.0 to 5.5 V vs Li^+/Li, the middle panel (b) shows the gases from the electro-oxidation of the EC-based electrolyte, $^{12}CO_2$ (purple lines) and ^{12}CO (purple dots), and the lower panel (c) shows the gases from electro-oxidation of the ^{13}C carbon electrode, $^{13}CO_2$ (magenta lines) and ^{13}CO (magenta dots). All gases are reported in units of μmol/m^2_C of carbon in the electrode. These units are obtained by converting the ppm gas concentration in our two-compartment OEMS cell (internal volume 8.5 ml) using the molar volume at the respective measurement temperature and normalizing to the total m^2 of carbon surface using

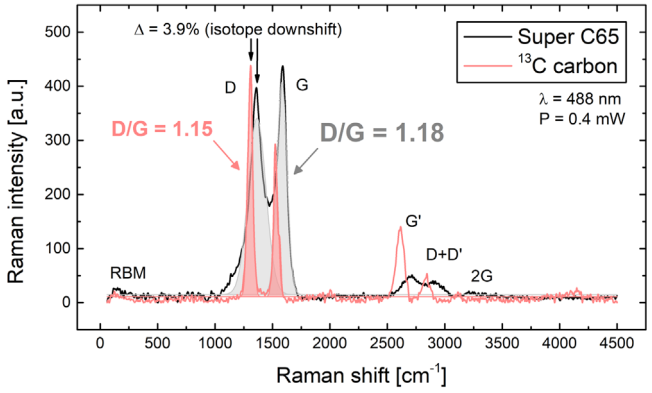

Figure 2. A Raman spectrum of Super C65 and the ^{13}C-labeled conductive carbon used in this work, showing a similar degree of graphitization according to the D/G integral ratio as well as the expected isotope downshift of 3.9% for ^{13}C carbon.

the loading (~1 mg cm^{-2} on a geometric area of 1.77 cm^2) and the BET surface area of the employed ^{13}C carbon (145 m^2 g^{-1}), amounting to ~0.026 m^2_C. We think that μmol/m^2_C is the most meaningful unit to describe intrinsic reaction rates, as it allows to compare gassing data from different research groups, which are typically obtained in custom cell hardware and with electrodes of variable loading or a different specific surface area on which oxidation reactions take place.

A closer look at Fig. 3b reveals that the anodic decomposition of EC in a $LiClO_4$-based electrolyte mainly yields $^{12}CO_2$ and some ^{12}CO via a minor reaction pathway. This is in agreement with our previous findings.[26] We recently suggested a reaction scheme for the anodic oxidation of EC with two pathways that lead to $^{12}CO_2$ and ^{12}CO, respectively.[19,37] We review these mechanisms in the Discussion section. As shown in Fig. 3c, the electro-oxidation of the ^{13}C-labled conductive carbon also yields both $^{13}CO_2$ and ^{13}CO in a $LiClO_4$-based electrolyte. Again, this is consistent with our previous study where the solvent in the electrolyte solution was isotopically labeled rather than the conductive carbon,[26] implying that switching this configuration around and labelling the carbon electrode is a viable alternative. In the fuel cell literature, carbon oxidation is usually rationalized by a reaction that involves water: $C + 2H_2O \rightarrow CO_2 + 4H^+ + 4e^-$ or $C + H_2O \rightarrow CO + 2H^+ + 2e^-$.[38] We investigated these reaction pathways in our previous study,[26] and demonstrated that H_2O addition to the carbonate electrolyte indeed enhances carbon oxidation (as well as electrolyte solution oxidation). Here, however, it is worth noting that the amount of $^{13}CO_2$ and ^{13}CO is higher than what could be rationalized by typical trace water contamination on the order of <20 ppm (as is the case for the present measurements). In fact, 20 ppm H_2O in the 240 μl of electrolyte (density 1.5 g cm^{-3}) in the working-electrode compartment could account for a maximum of 1.4 μmol/m^2_C of $^{12}CO_2$, assuming the above reaction equation, which is ~2.5-fold lower than the amount of $^{12}CO_2$ obtained at the end of the LSV experiment conducted at 50 °C shown in Fig. 3b. In the Discussion section we identify an alternative oxygen source for carbon oxidation. Note that our proposed EC oxidation mechanism does not require the presence of H_2O.[19]

Figure 3 demonstrates also that both reactions, the electro-oxidation of the electrolyte solution and carbon, are temperature and potential dependent. At room temperature both reactions have an onset at ~5 V vs Li$^+$/Li. At 50 °C, CO and CO_2 evolution start already at ~4.5 V vs Li$^+$/Li. This is an interesting finding with regards to high-voltage spinel cathodes (operating at an average potential of ~4.8 V vs Li$^+$/Li). This cathode material usually works well with standard carbonates based electrolyte solutions at room temperature but shows strong capacity fading at elevated temperatures.[37,39]

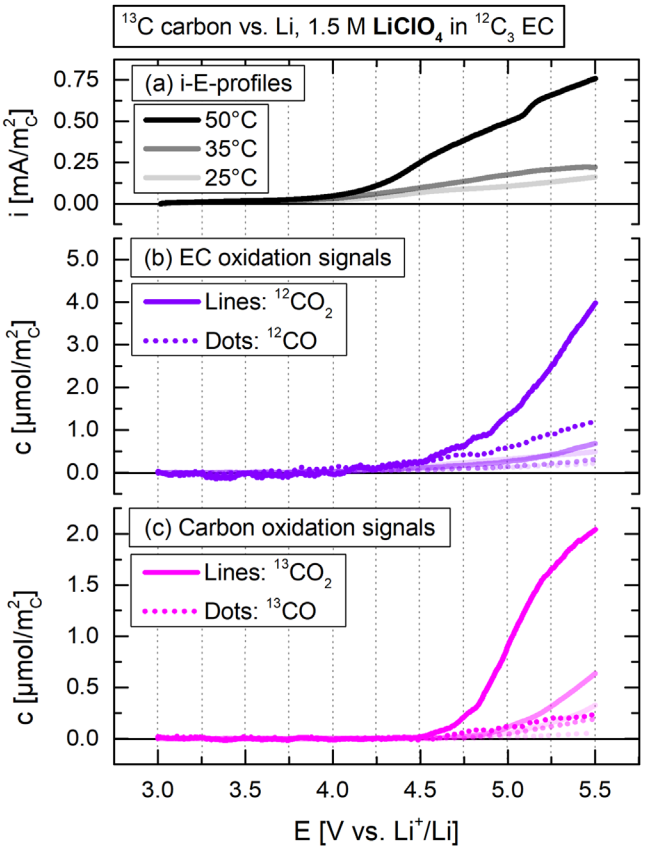

Figure 3. (a) Linear potential sweep to 5.5 V vs Li$^+$/Li of a PVdF-bonded ^{13}C carbon electrode vs metallic lithium in a two-compartment cell containing 1.5 M $LiClO_4$ in EC. (b) Corresponding $^{12}CO_2$ and ^{12}CO evolution from EC oxidation, and, (c) corresponding $^{13}CO_2$ and ^{13}CO evolution form carbon oxidation. The measurement was done at 25 °C, 35 °C, 50 °C and 60 °C (latter not shown) as indicated by transparency level; CO_2 is shown as solid lines, CO is shown as dots.

Figure 4 reveals a completely different picture for the 1.5 M $LiPF_6$ $^{12}C_3$ EC-based electrolyte solution. The solution (in fact EC) oxidation clearly scales with temperature and gives an overall similar amount of $^{12}CO_2$ as in the case of $LiClO_4$, however, there is very little ^{12}CO from EC oxidation with $LiPF_6$, even at 50 °C (see Fig. 4b). Accordingly, the EC oxidation pathway that leads to CO seems to be strongly suppressed with $LiPF_6$ and not influenced by temperature. More striking is the fact that there is almost no carbon oxidation with $LiPF_6$ up to 5.25 V vs Li$^+$/Li (see Fig. 4c). This means that conductive carbon is actually fairly stable in ethylene carbonate-based electrolyte solution if $LiPF_6$ is used as the lithium salt, even at 50 °C. The absence of carbon oxidation for $LiPF_6$ is consistent with the finding by Abarbanel et al.[28] that electronic resistances in an NMC442 cathode cycled to ~4.6 V vs Li$^+$/Li in a $LiPF_6$-based electrolyte at 25 °C are a minor contributor to the overall impedance growth at high voltage. It is also consistent with the observation that the build-up of an electronic contact resistance between an LNMO cathode and the aluminum current collector upon extended cycling of an LNMO/graphite cell at 40 °C in an $LiPF_6$-based electrolyte was shown to be due to the formation of an insulating surface film on the current collector rather than to carbon corrosion.[29] We discuss further both of these $LiPF_6$ related phenomena, viz., the absence of CO from EC oxidation and the absence of carbon oxidation, in the Discussion section.

The same anodic stability experiments were done with LiTFSI and $LiBF_4$ as conducting salts in EC-based electrolyte solution , showing both very low carbon and electrolyte solution oxidation at 25 °C and 35 °C (see Figs. S1 and S2, which are available online at

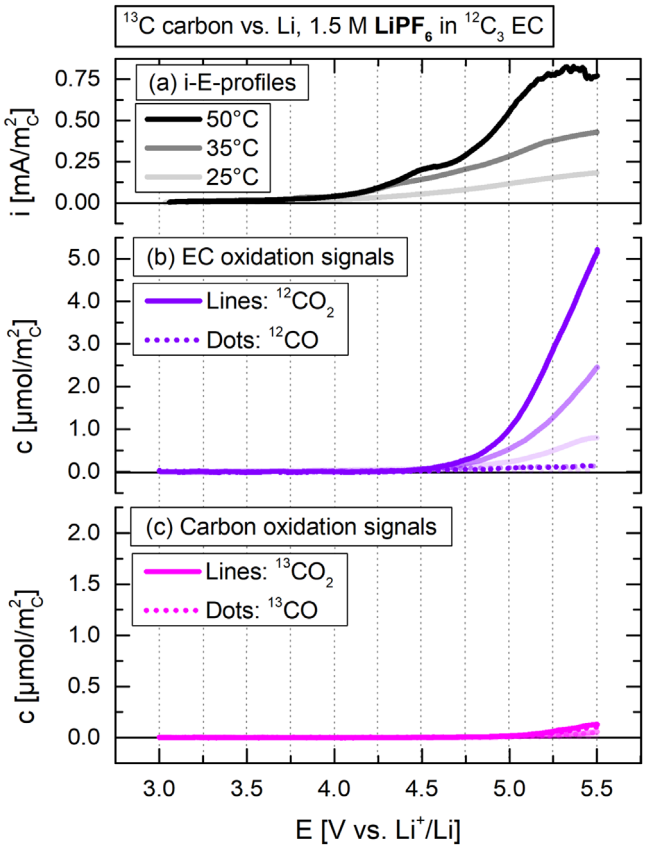

Figure 4. (a) Linear potential sweep to 5.5 V vs Li^+/Li of a PVdF-bonded ^{13}C carbon electrode vs metallic lithium in a two-compartment cell containing 1.5 M $LiPF_6$ in EC. (b) corresponding $^{12}CO_2$ and ^{12}CO evolution from EC oxidation, and, (c) corresponding $^{13}CO_2$ and ^{13}CO evolution form carbon oxidation (c). The measurement was done at 25 °C, 35 °C, 50 °C and as indicated by transparency level; CO_2 is shown as solid lines, CO is shown as dots.

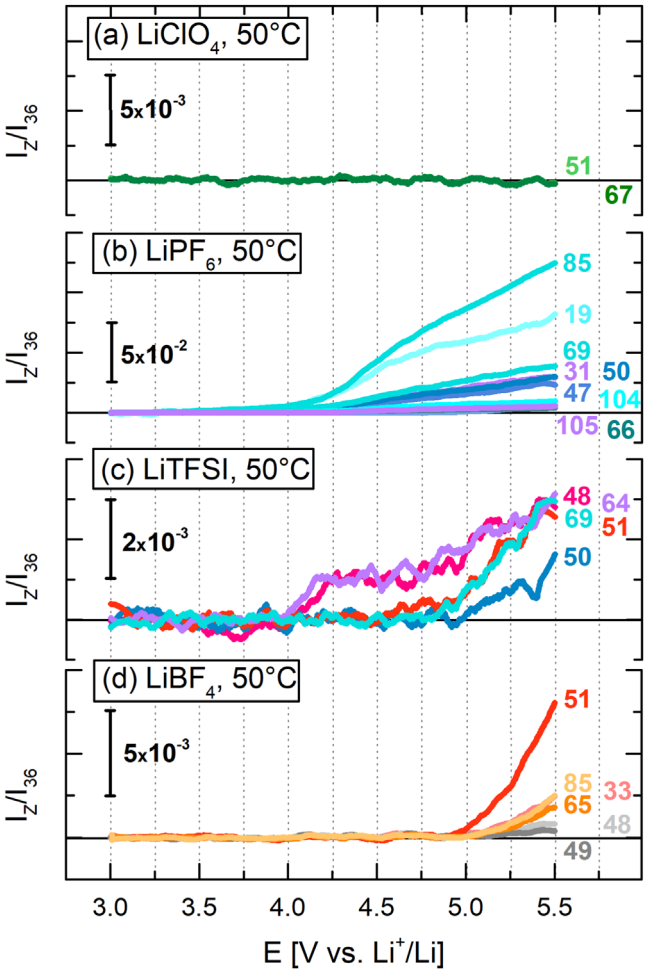

Figure 5. Evolution of mass signals other than CO_2 and CO during a linear potential sweep to 5.5 V vs metallic lithium of a PVdF-bonded ^{13}C carbon electrode in a two-compartment cell at 50 °C with EC-based electrolyte containing either 1.5 M $LiClO_4$ (a), $LiPF_6$ (b), LiTFSI (c), or $LiBF_4$ (d). The mass signals are baseline corrected and shown with their ion current I_Z normalized to the ion current I_{36} of the Ar background.

stacks.iop.org/JES/167/160522/mmedia in the Supplementary Information and Fig. 7 for a summary of the results). At 50 °C there is electrolyte solution oxidation with both salts, but at lower levels than for $LiClO_4$ and $LiPF_6$. Carbon oxidation at 50 °C is very low for LiTFSI and moderate for $LiBF_4$. Since we summarize the oxidation rates of carbon and electrolyte solution when we present the kinetic analysis in the Discussion section (see Fig. 7), we do not show the raw data for LiTFSI and $LiBF_4$.

Gaseous products from side reactions of lithium salts.—Prior to a kinetic analysis, we should look at all mass signals other than CO and CO_2 observed in the OEMS experiments, as this could allow for a better understanding of the anodic stability of the conducting salts and the type of side reactions that these salts undergo. Figure 5 depicts these mass signals for the linear potential sweeps to 5.5 V vs Li^+/Li at 50 °C with $LiClO_4$ (a), $LiPF_6$ (b), LiTFSI (c), and $LiBF_4$ (d). Apart from the already discussed CO_2 and CO isotopes, no additional mass signals are observed for $LiClO_4$ (see Fig. 5a). This implies that the anodic oxidation of EC and carbon with $LiClO_4$ are very "clean" reactions, involving no side reactions with the lithium salt to form, e.g., ClO_2 as suggested by Cattaneo and Ruch.[40] These authors stated that the oxidation of the perchlorate anion would lead to the evolution of ClO_2 (main signals m/z = 67, 51)[41] via $ClO_4^- \rightarrow ClO_2 + 2O_{(ads)} + e^-$. This reaction can be ruled out due to the absence of any ion current signals on m/z = 67 and 51, as shown in Fig. 5a. It is important to point out that the absence of gaseous byproducts does not mean that there are no byproducts at all. In fact, we later present an XPS analysis of the carbon surface before and after polarization to 5.5 V vs Li^+/Li in an attempt to look for solid reaction products.

The oxidative scan with $LiPF_6$ at 50 °C shown in Fig. 5b exhibits a variety of gaseous byproducts that can be identified as follows: (i) POF_3, with a theoretical fragmentation pattern (m/z [%signal]) of 104 [100%], 85 [80%], 69 [20%], 50 [<10%], 47 [<10%], 88 [<5%],[17,42] (ii) HF on m/z = 19 (the main HF signal on m/z = 20 cannot be quantified due to the large background signal from Ar in the cell head space on channels m/z = 40 and 20), and (iii) other signals which cannot be unambiguously identified at this point (m/z = 31, 105). Cattaneo et al.[43] ascribed the signals on m/z = 31 to carbonyl fluoride COF_2, which has a fragmentation pattern that would match our data, 47 [100%], 66 [55%], 28 [14%], 31 [4%].[44] Here it should be noted that the relative intensities of the various m/z-signals obtained in our OEMS setup generally differ from those given in the NIST data base, particularly for the signals from larger molecular fragments, which is due to the fact that the mass spectrometer of our OEMS setup is thermostated at 100 °C[32] (rather than at 25 °C where the NIST data are recorded), which typically suppresses the intensity of large molecular fragments produced by the electron-beam ionization.

The observed gaseous byproducts we have detected suggest that $LiPF_6$ as a conducting salt causes strong side reactions at high temperature and high voltage, whereby the data in Fig. 5b suggest that POF_3 and HF are the main reaction products (m/z = 85, 19, 69,

50). At 50 °C, the onset voltage of POF_3 formation is as low as 4.0 V vs Li^+/Li. This is ~200 mV lower than the onset voltage of POF_3 at 25 °C measured in a similar experiment in our previous study,[14] which makes sense given the temperature difference. The ion current of the most intense signal m/z = 85 normalized to the Ar signal on m/z = 36, written as I_{85}/I_{36}, amounts to $\sim 8 \times 10^{-2}$ at 5.0 V vs Li^+/Li. This number can be converted into a POF_3 concentration of ~940 ppm with the calibration factor determined in our previous study.[14] It is in reasonably good agreement with the ~750 ppm of POF_3 observed in the analogous experiment conducted by Solchenbach et al. with a carbon electrode of lower surface area at 25 °C.[14] For comparison, the $^{12}CO_2$ signal from electrolyte oxidation in the measurement with $LiPF_6$ at 50 °C and 5.0 V vs Li^+/Li is ~1 $\mu mol/m^2_C$ which corresponds to a concentration of ~800 ppm in our cell hardware. Thus, at 50 °C and 5.0 V vs Li^+/Li, POF_3 and $^{12}CO_2$ are found at approximately equal concentrations; however, the $^{12}CO_2$ signal increases exponentially with the applied potential, whereas POF_3 seems to level off. While POF_3 was previously reported to stem from the reaction of H_2O impurities in the carbonate based electrolyte solution reacting with $LiPF_6$ (see Eq. 1),[13,45] it is important to note that this mechanism is not suitable to explain the strongly potential driven POF_3 evolution in our experiment (see Discussion section).

$$H_2O + LiPF_6 \rightarrow LiF + 2HF + POF_3 \quad [1]$$

As a matter of fact, the POF_3 evolution does not set in unless the potential of the working electrode is higher than ~4.0 V vs Li^+/Li. The detection of corrosive POF_3 and HF for $LiPF_6$ at high voltage is consistent with the significant discolorations observed by Ellis et al. of the separator and the electrode tape from the outside of the jelly roll in pouch cells with $LiPF_6$.[16] In the Discussion section we further investigate the origin of the POF_3 signal that is detected by OEMS.

The linear potential sweep with 1.5 M LiTFSI in EC (Fig. 5c) shows low intensity signals on m/z = 64, and 48. These signals can be identified as SO_2 from the $TFSI^-$ anion (see Fig. 1c). The remaining signals m/z = 69, 51, 50 likely derive from HCF_3[46] that might form upon decomposition of the $TFSI^-$ anion to SO_2 and other fragments that react to HCF_3 in the presence of protic species that are produced by EC oxidation.[19] The onset voltages of the two different signal groups in Fig. 5c suggest that the SO_2 moieties come off already at relatively low voltages of ~4.0 V vs Li^+/Li, while the HCF_3 group is evolved only above 4.75 V vs Li^+/Li. It has to be pointed out, however, that the intensity of the signals is ~25-fold smaller than for $LiPF_6$ (compare Figs. 5b and 5c), such that the overall anodic stability of the LiTFSI salts can be classified as significantly higher. Due to the high stability of LiTFSI, the Al current collector at the positive electrode is known to be insufficiently passivated when LiTFSI is the main electrolyte salt, which renders it unsuitable as a single lithium salt in lithium-ion batteries.[9,10,47]

The anodic scan with $LiBF_4$ containing electrolyte solution also shows distinct gaseous byproducts in OEMS with mass signals on m/z = 51, 85, 65, and 33. While some of these signals could be ascribed to fragments of the PVdF binder, e.g., CHF_2 (m/z = 51) or CH_2F (m/z = 33), the PVdF binder was demonstrated to be stable up to 5.5 V vs Li^+/Li in $LiClO_4$-based electrolyte (see Fig. 13 in Ref. 26), so that we consider this an unlikely assignment. As stated by Cattaneo et al.,[43] fluorinated species could also stem from a reaction of BF_4^- ions with oxidized carbonate solvents (in their case propylene carbonate), yielding, e.g., 1,1-difluoroethane with the fragmentation pattern 51 [100%], 65 [50%], 47 [9%], 15 [4%].[48] BF_3, the expected gaseous decomposition product of the $LiBF_4$ conducting salt, was only detected in marginal quantities on channels m/z = 48 and 49. Again, it has to be pointed out that the signals detected for $LiBF_4$ are one order of magnitude smaller than the ones for $LiPF_6$. This indicates a high anodic stability of the salt, which is in line with results presented by Ellis et al.,[16] who found via impedance spectroscopy, ex situ XPS of harvested electrodes, and impedance measurements of positive/positive symmetric cells assembled from harvested electrodes that the use of $LiBF_4$ leads to less side reactions at high voltage than the use of $LiPF_6$.

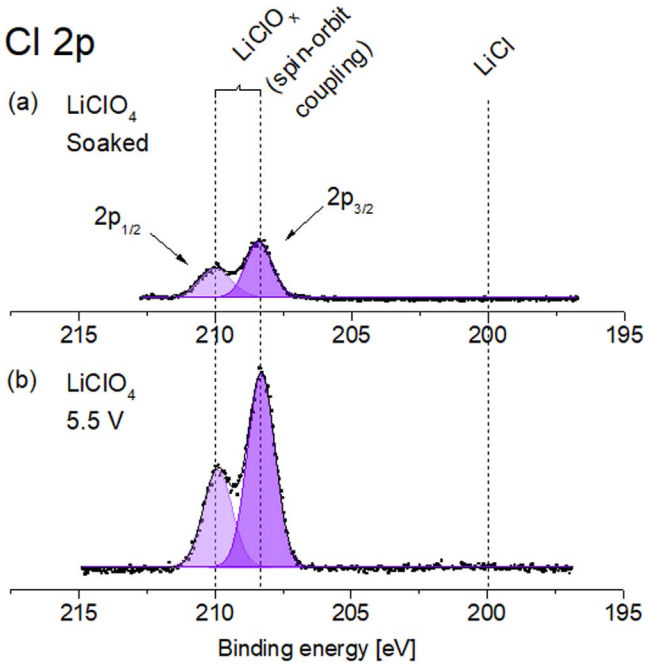

Figure 6. Cl 2p XPS spectra of a grafoil working-electrode soaked in 1.5 M $LiClO_4$ EC electrolyte (a) or polarized to 5.5 V vs a metallic lithium counter-electrode at 25 °C in the same electrolyte (b).

Solid products from side reactions of lithium salts.—As the linear sweep voltammogram at 50 °C with $LiClO_4$ (see Fig. 5a) did not show any gaseous reaction products apart from CO and CO_2, we use XPS to look for solid reaction products. Figure 6 depicts the Cl 2p spectra for a grafoil working-electrode that was soaked in 1.5 M $LiClO_4$ EC solution (a) and a grafoil working-electrode that had been subjected to the same LSV 5.5 V vs Li^+/Li that was used for the OEMS experiments in the same electrolyte (b). The spectra of the soaked grafoil electrode exhibits $LiClO_x$ signals with $2p_{1/2}$ and $2p_{3/2}$ doublets at 210 and 208 eV, respectively.[49] This is most likely residual $LiClO_4$ that was not removed during washing. The polarized electrode shows a stronger $LiClO_x$ signature, which suggests that at least on a semi-quantitative basis more residual salt species are present. This could be the case, if $LiClO_4$ were to contribute one or more oxygen atoms to oxidize the conductive carbon to CO_2 and CO (see Eqs. 2 and 3).

$$LiClO_4 + 1/2\,^{13}C \rightarrow LiClO_3 + 1/2\,^{13}CO_2 \quad [2]$$

$$LiClO_4 + {}^{13}C \rightarrow LiClO_3 + {}^{13}CO \quad [3]$$

The transition from lithium perchlorate to lithium chlorate and oxygen in a first step in these reactions would have a negative free energy change of $\Delta G = -143\ kJ\ mol^{-1}$, according to a simple thermochemistry calculation. The clear absence of a LiCl signal at 200 eV rules out a full oxidation of the salt to produce lithium chloride and molecular oxygen.[49] In summary, the comparison of the Cl 2p spectra suggests that the strong oxidant $LiClO_4$ could serve as a potential oxygen source for carbon oxidation. XPS spectra of pristine and polarized grafoil electrodes with the other salts revealed (i) surface LiF for $LiPF_6$, (ii) SO_2 surface species for LiTFSI, and (iii) $Li_xBO_yF_z$ species for $LiBF_4$ (see Figs. S5–S13 for XPS spectra and Tables SI–SIII for peak assignments in the Supplementary Information).

Discussion

Oxidation rates of conductive carbon and EC for different lithium salts.—In this section we use the CO_2 and CO evolved during the electro-oxidation of the ^{13}C-labeld conductive carbon and of the ethylene carbonate (see Results section) to compute the respective oxidation rates for the different lithium salts. A similar analysis was done in our previous work.[26] The interested reader is encouraged to study the details of the procedure there. In short, we sum up the respective amounts of CO_2 and CO evolved during an isothermal LSV experiments due to either EC oxidation (i.e., $^{12}CO_2$ + ^{12}CO) or carbon oxidation (i.e., $^{13}CO_2$ + ^{13}CO), and perform a linear fit of the data in a narrow potential window (±50 mV) around 5.0 V vs Li^+/Li to determine the slope and thus the approximate time derivative of the respective $^xCO_2$ + ^xCO curve (see Fig. S3). We then convert the data into a surface area normalized molar oxidation rate in units of [$mol_{CO2+CO}/(s{\cdot}m^2_C)$], and plot it in an Arrhenius-type graph. In lithium-ion cells, such rates would likely be seen if a cell had a high-voltage cathode that operates for a significant fraction of its operational time above the threshold voltage for electrochemical carbon or electrolyte oxidation, e.g., $LiNi_{0.5}Mn_{1.5}O_4$ (LNMO, 2nd plateau at ~4.8 V vs Li^+/Li)[37] or $LiCoPO_4$ (LCP, most of charge >4.8 V vs Li^+/Li).[50,51] Our analysis is also relevant for storage of high-voltage battery cells at high state-of-charge, i.e., high cell voltage, where in principle the cathode potential can be above the threshold voltage for electro-oxidation of carbon or electrolyte.

Figure 7 shows the results of this analysis for carbon (magenta squares) and ethylene carbonate (purple triangles). For all lithium salts, the oxidation rates at 5.0 V vs Li^+/Li are increasing strongly with temperature. For $LiClO_4$ (Fig. 7a), the oxidation rates of carbon and EC are almost identical, with slightly different temperature dependencies, as indicated by the dashed lines in Fig. 7a that are an Arrhenius fit to the data (discussed later on). From 25 °C to 60 °C, the rate of carbon oxidation increases by a factor of ~17 (from ~$2.9{\cdot}10^{-11}$ mol/($s{\cdot}m^2_C$) to ~$0.50{\cdot}10^{-9}$ mol/($s{\cdot}m^2_C$)) while the EC oxidation rate increases by a slightly higher factor of ~24 (from ~$4.1{\cdot}10^{-11}$ mol/($s{\cdot}m^2_C$) to $1.0{\cdot}10^{-9}$ mol/($s{\cdot}m^2_C$)). This large increase of the oxidation rates from 25 °C to 60 °C shows that the oxidation reactions in lithium-ion batteries are strongly temperature activated processes, which of course is challenging when aiming to achieve stable cycle life for batteries operating at high-voltage and elevated temperatures.[52] The oxidation rates obtained herein for EC with 1.5 M $LiClO_4$ and the ^{13}C-labeled conductive carbon can be compared with those acquired in our previous work[26] in the same electrolyte solution but with Super C65 conductive carbon (BET surface area of 68 $m^2\ g^{-1}$). In that work, the oxidation rates at 5.0 V vs Li^+/Li had been given in units of mol/($s{\cdot}g_C$), which when multiplied by the Super C65 BET surface area convert to the units of mol/($s{\cdot}m^2_C$) used herein. The oxidation rates thus obtained for the Super C65 carbon (~$2.8{\cdot}10^{-11}$ mol/($s{\cdot}m^2_C$) at 25 °C and ~$0.52{\cdot}10^{-9}$ mol/($s{\cdot}m^2_C$) at 60 °C) are in perfect agreement with the oxidation rates obtained for the ^{13}C-labeld carbon in this study. This finding supports well our assumption based on the analysis of the Raman spectra (Fig. 2) that the electro-oxidation stability of these two carbons should be very similar. While the oxidation rates of the EC were ~1.5-fold higher in our previous work where we used $^{13}C_3$ labeled EC (~$6.0{\cdot}10^{-11}$ mol/($s{\cdot}m^2_C$) at 25 °C and ~$1.6{\cdot}10^{-9}$ mol/($s{\cdot}m^2_C$) at 60 °C), the agreement is still quite reasonable.

Figure 7b shows the oxidation rates of carbon and EC when using $LiPF_6$ as the lithium salt. For $LiPF_6$, no measurements were done at 60 °C in order to avoid the interference by possible other reactions triggered by the thermal decomposition of $LiPF_6$, as it has a well-known limited stability at high temperatures.[45] However, over the investigated temperature range, the electro-oxidation of the EC is by far the dominating reaction. With $LiPF_6$, the oxidation rates of the EC at 5.0 V vs Li^+/Li are essentially the same as those obtained with $LiClO_4$ (to aid this comparison, the dashed purple line in Fig. 7b represents the Arrhenius fit of the electrolyte oxidation rates with 1.5 M $LiClO_4$ from Fig. 7a). On the other hand, the oxidation rates of the ^{13}C conductive carbon are almost two orders of magnitude lower in $LiPF_6$-based compared to $LiClO_4$-based electrolyte solutions (again, for ease of comparison, the dashed magenta line in Fig. 7b represents the Arrhenius fit of the electrolyte oxidation rates with 1.5 M $LiClO_4$). This means that carbon is practically stable even at 5.0 V vs Li^+/Li with $LiPF_6$ as the lithium salt.

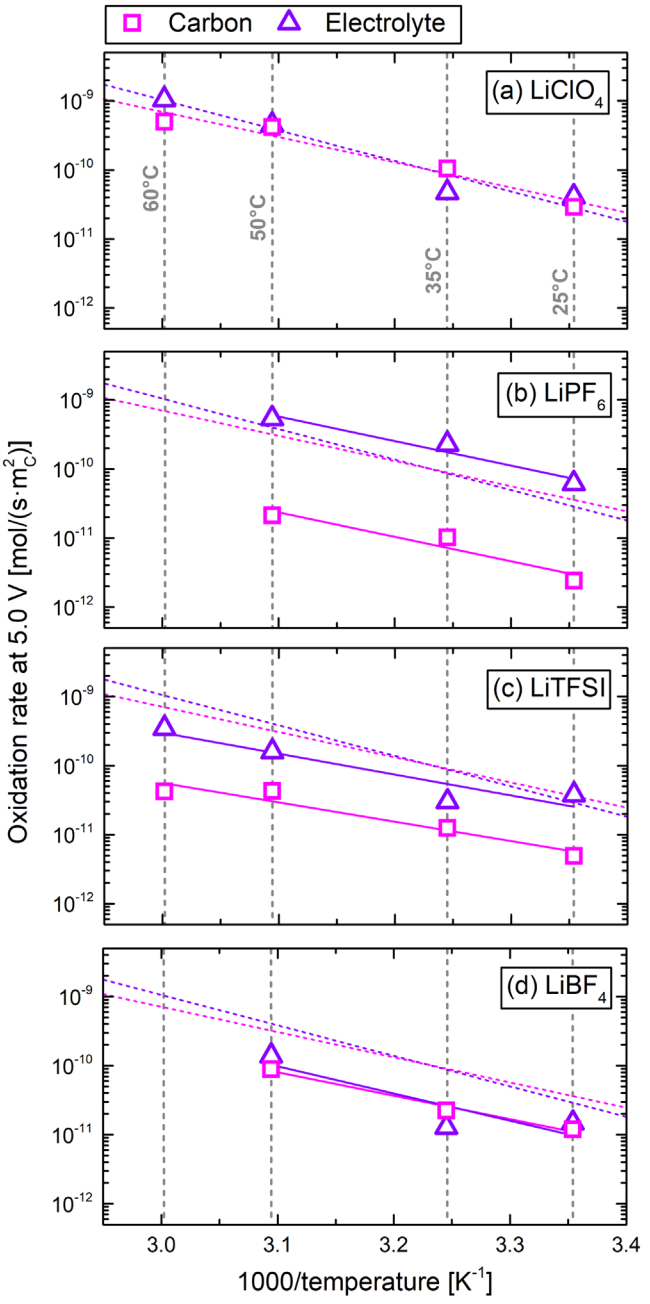

Figure 7. Arrhenius plots of the electro-oxidation rates at 5.0 V vs Li^+/Li of the ^{13}C-labeled conductive carbon and of the $^{12}C_3$ EC electrolyte for the different lithium salts: $LiClO_4$ (a), $LiPF_6$ (a), LiTFSI (c), and $LiBF_4$ (d). All salts are dissolved at 1.5 M in EC. The molar electro-oxidation rates are normalized to the total surface area of the ^{13}C carbon electrode. The rate is determined at 25 °C, 35 °C, and 50 °C for all salts, while for the thermally more stable salts $LiClO_4$ and LiTFSI additional data are provided at 60 °C. The dashed/solid lines represent Arrhenius fits of the data, which were used to determine the apparent activation energies listed in Table I. Please note that the dashed lines representing the Arrhenius fits for the rates in the $LiClO_4$-based electrolyte in panel (a) are also added to the other panels to serve as reference.

Table I. Apparent activation energies for carbon and electrolyte solution (EC) oxidation extracted from the slopes of the linear regression lines in the Arrhenius plots of Fig. 7.

Salt	Apparent activation energy [kJ mol^{-1}]	
	Carbon oxidation	Electrolyte oxidation
$LiClO_4$	69	84
$LiPF_6$	68	68
LiTFSI	54	58
$LiBF_4$	65	75

As shown in Fig. 7c, the oxidation rates at 5.0 V vs Li^+/Li of the electrolyte solution with LiTFSI as the lithium salt are lower than those measured with $LiClO_4$ (~1.5-fold) and $LiPF_6$ (~3-fold) solutions. Furthermore, over the whole temperature range from 25 °C to 60 °C, the carbon oxidation rates are about one order of magnitude lower than that of the electrolyte solution oxidation (namely, EC) rates and ~2-fold higher than in the $LiPF_6$-based electrolyte. Nevertheless, the carbon oxidation rates with LiTFSI are still more than an order of magnitude lower than with $LiClO_4$.

Interestingly, the use of $LiBF_4$ leads to low oxidation rates for both carbon and EC (see Fig. 7d). In fact, $LiBF_4$ shows the lowest electrolyte solution oxidation rates of the four lithium salts investigated in this study; over the temperature range from 25 °C–50 °C, the electrolyte solution oxidation rates are ~4-fold lower for $LiBF_4$ compared to $LiPF_6$. This finding is consistent with the reports by Dahn's group, who compared the performance of NMC442/graphite cells cycled to 4.35 V and of NMC442/NMC442 symmetric cells at 40 °C with 1 M $LiBF_4$ or 1 M $LiPF_6$ in EC:EMC (3:7 g:g), showing that for pure $LiBF_4$ salt, less gassing was observed during formation, the impedance growth at the cathode was reduced, and more stable cycling was attained for NMC442/NMC442 symmetric cells.[16,30] This all points towards higher oxidative stability of $LiBF_4$ compared to $LiPF_6$, consistent with the data in Fig. 7.

Interpolating the data points in the Arrhenius plots (Fig. 7) by a linear regression fit, the slopes represent the apparent activation energies for carbon and EC oxidation with the four different lithium salts and are summarized in Table I. The ~69 kJ mol^{-1} for carbon oxidation in an $LiClO_4$ electrolyte are in reasonably good agreement with the ~65 kJ mol^{-1} that were obtained in our previous study where the EC was isotopically labeled and regular Super C65 carbon was employed.[26] The apparent activation energy for carbon oxidation with $LiClO_4$ is also quite similar to the apparent activation energy of ~67 kJ mol^{-1} for carbon oxidation in fuel cells.[38,53] The apparent activation energy for EC oxidation of ~84 kJ mol^{-1} found in this study, however, is lower than in our previous measurements with isotopically labeled EC and Super C65 carbon (~104 kJ mol^{-1}),[26] the origin of which is not clear, but may be due to the wider temperature range that had been used in our former study (10 °C–60 °C). Comparing the apparent activation energies for electrolyte oxidation vs carbon oxidation for each lithium salt, they differ by a maximum of ~20%, which is probably within the accuracy of our measurements, considering the rather narrow temperature window (25 °C–50 °C for $LiPF_6$ and $LiBF_4$ and 25 °C–60 °C for $LiClO_4$ and LiTFSI).

Projected conductive carbon and electrolyte solution weight loss at 5.0 V vs Li^+/Li.—The molar oxidation rates given in Fig. 7 stem from CO_2 and CO that are evolved from electro-oxidation of the electrolyte solutions and the conductive carbon. Consequently, solvent molecules and carbon particles get consumed and the gases are a direct way to quantify this consumption. For the electrolyte solutions these numbers represent a lower limit, as the electrolyte solution can also be lost to solid or liquid reaction products. In order to put the above determined oxidation rates of ethylene carbonate-based electrolyte solutions and conductive carbon into perspective, we further calculated the weight loss that would be associated with these oxidation rates, if a battery was stored at 5.0 V vs Li^+/Li for 100 h. Such an analysis was already done for $LiClO_4$ in our previous article, in which a detailed description can be found.[26] Thereby, here we outline the principle of this analysis only briefly.

We assume that the active-material (AM) in the cathode does not have any catalytic activity for electro-oxidation of the carbon or the electrolyte solution, i.e., the decomposition rate is simply proportional to the overall surface area in the electrode.[20] Further, we do not consider the chemical electrolyte solution decomposition pathway via singlet oxygen released from layered oxide cathodes that occurs at delithiation degrees of approximately >80% for layered transition metal oxides (e.g., NMC type cathodes).[11,54] We also assume that the total surface area of the active-material is small compared to that of the conductive carbon (here we use 68 m^2 g^{-1}, the surface area of common Super C65 carbon, rather than the 145 m^2 g^{-1} of our ^{13}C carbon, such that for a typical battery cathode composed of 90 wt.% cathode AM at 1 m^2 g^{-1} and 5 wt.% Super C65 at 68 m^2 g^{-1}, ~80% of the total surface area are that of the carbon). Under these assumptions, the carbon weight-normalized ethylene carbonate oxidation rates given in Fig. 7 provide a reasonable estimate for the oxidation rate in a typical battery cathode. According to Wagner et al.,[55] the weight ratio of the electrolyte solution and the cathode active-material in a typical battery is ~0.35/1 $g_{electrolyte}/g_{AM}$, which for an assumed conductive carbon content of 5 wt.% results in an electrolyte to carbon ration of ~7/1 $g_{electrolyte}/g_C$. By dividing the electrolyte solution oxidation rates in Fig. 7 by the $g_{electrolyte}/g_C$ ratio and by multiplying the latter by the molecular weight of EC (88 g mol^{-1}), one obtains the fractional EC loss rate. In summary, the equations for calculating the carbon and electrolyte solutions weight loss extrapolated from these initial rates over a time of 100 h, Λ_C and Λ_{EC}, are:

$$\Lambda_C[\text{wt.\%}_C/100\text{ h}] = r_C[\text{mol}/(\text{m}^2_C \cdot \text{s})] \cdot 3.6 \cdot 10^5\text{ s} \cdot 68\text{ m}^2_C/g_C \cdot 12\text{ g}_C/\text{mol}_C \cdot 100 \quad [4]$$

$$\Lambda_{EC}[\text{wt.\%}_{EC}/100\text{ h}] = r_{EC}[\text{mol}/(\text{m}^2_C \cdot \text{s})] \cdot 3.6 \cdot 10^5\text{ s} \cdot 68\text{ m}^2_C/g_C/(7\text{ g}_{EC}/g_C) \cdot 88\text{ g}_{EC}/\text{mol}_{EC} \cdot 100 \quad [5]$$

The weight losses thus projected over 100 h at 5.0 V vs Li^+/Li are reported in Fig. 8. Figure 8a illustrates that a considerable fraction of conductive carbon and electrolyte solution is lost with an electrolyte solution comprising $LiClO_4$ as the lithium salt, especially at elevated temperature. While the weight loss of both components is still acceptable at low temperature (<5 wt.% at 25 °C and 35 °C, respectively), it becomes substantial at 50 °C, where >10 wt.% of the carbon and the solvent in the battery would be lost as CO_2 and CO. At 60 °C, ~1/3 of the electrolyte solution would be consumed within 100 h at 5.0 V. The current measurements and projections with $LiClO_4$ suggest that carbon oxidation at high temperature and potential should be substantial, as we had concluded in our previous work.[26]

Remarkably, with $LiPF_6$ the low oxidation rates of the conductive carbon (see Fig. 7b) lead to almost no projected carbon weight loss over 100 h at 5.0 V, even at 50 °C (see Fig. 8b). On the other hand, the projected loss of solvent (EC) is severe with $LiPF_6$ already at 35 °C, reaching a projected electrolyte loss over 100 h at 5.0 V of 17 wt.% at 50 °C. Electrolyte solution losses (mostly the solvents component) on that order of magnitude are consistent with the observation that cells cycled at high voltage and elevated temperature are often found to dry out.[52,56] Such cells show a build-up of thick resistive layers of decomposition products[27] and acidification of the electrolyte solution, as protons are being generated.[19,47] The latter can cause H_2 gassing by a crosstalk with the anode[19] as well as dissolution of transition metals from the cathode by HF attack.[12,21,22] While CO_2 was shown to be consumed at the anode side,[57–59] the

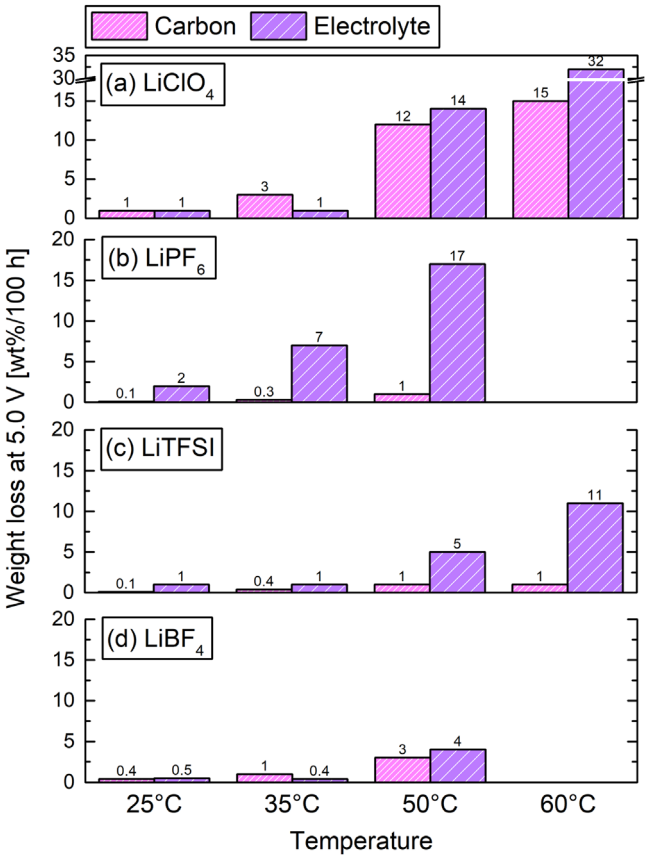

Figure 8. Projected weight losses over 100 h at 5.0 V vs Li^+/Li of conductive carbon (projected for Super C65 with 68 m^2 g^{-1} BET) and electrolyte for EC electrolytes with $LiClO_4$ (a), $LiPF_6$ (a), LiTFSI (c), and $LiBF_4$ (d). The weight loss is calculated from the rates shown in Fig. 7 that were determined at 25 °C, 35 °C, and 50 °C for all salts, with additional data at 60 °C for the thermally more stable salts $LiClO_4$ and LiTFSI.

sheer amount of gases produced at such high voltages would likely lead to swelling of pouch bag cells or inhomogeneous current distributions and lithium dendrites due to formation of gas bubbles between the electrodes.[60]

The use of LiTFSI is projected to lead to quite low overall weight losses of conductive carbon over 100 h at 5.0 V even at 60 °C (only ~1 wt.%), and even the projected electrolyte loss remains at ~1 wt.% at 35 °C and only reaches 5 and 11 wt.% at 50 and 60 °C, respectively. This would render LiTFSI a good candidate for high-voltage cells, however, (salt) additives would be needed to provide a sufficient passivation of the aluminum current collector.[9]

In the case of $LiBF_4$-based electrolyte, the projected stability of the conductive carbon and the electrolyte over 100 h at 5.0 V is quite exceptional compared to the other lithium salts. At 25 °C and 35 °C, essentially no weight loss is projected. At 50 °C, the weight loss of the conductive carbon and the EC amount to 3 and 4 wt.%, respectively. Maybe these numbers could be lowered by using optimized electrode solutions/additives in real battery cells, although, recent work by Dahn's group showed that a 2 M $LiBF_4$ electrolyte solution by itself already outperforms the best $LiPF_6$-based electrolyte solutions' formulations with additives.[31]

Mechanistic considerations.—Finally, we summarize a few thoughts on the distinct differences between $LiClO_4$ and $LiPF_6$ in terms of electrolyte solution and conductive carbon stability. The main observations made in the Results sections were: (i) almost no carbon oxidation with $LiPF_6$ (see Fig. 4c) in contrast to the strong carbon oxidation observed with $LiClO_4$ solutions (see Fig. 3c), (ii) almost no CO generation from electrolyte solution oxidation with $LiPF_6$ (see Fig. 4b), and (iii) strong POF_3 and HF OEMS mass signals with $LiPF_6$, while $LiClO_4$ showed no gaseous side products (see Figs. 5a and 5b). Clearly, an oxygen source is needed for the oxidation of carbon and the generation of POF_3 that is detected by OEMS.

Let us first discuss the differences in the carbon oxidation rates (deduced from the evolution of ^{13}CO and $^{13}CO_2$) with $LiPF_6$ vs $LiClO_4$ as lithium salts. In $LiClO_4$-based electrolyte solutions, oxygen can be provided from the conducting salt, as $LiClO_4$ is known to be a strong oxidant and as the XPS data indicate the presence of $LiClO_x$ surface species (see Fig. 6). Thus, it is not surprising that strong carbon oxidation is observed with $LiClO_4$ as lithium salt. When using $LiPF_6$, the only oxygen source in the system is the ethylene carbonate solvent. Jung et al.[11] previously suggested that the chemical oxidation of EC with reactive oxygen released from the near-surface region of layered transition metal oxide based cathode active-materials (singlet oxygen, as later proven by Wandt et al.[54]) can generate H_2O in addition to CO_2 and CO. However, here we only have the pure electro-oxidation of EC on a carbon surface (which, of course, cannot release oxygen at high potentials). So, we can rule out the in situ generation of H_2O as an oxygen source. Considering the previously identified oxidation pathways of EC in the absence of O_2 release,[14,17,61] it is difficult to conceive of a feasible EC oxidation mechanism that would provide oxygen for subsequent carbon oxidation, as most oxygen contained in the EC molecule is transformed to CO_2 or CO. Thus, it is not surprising that the carbon oxidation rates with $LiPF_6$ are very small compared to the EC oxidation rates, and the small ^{13}CO and $^{13}CO_2$ formation rates with $LiPF_6$ as lithium salt must be due to minor side reactions and/or minor impurities in the electrolyte solution or on the carbon surface.

We now, however, have to address the puzzling observation that POF_3, another oxygen containing gas, is detected by the mass spectrometer in substantial quantities in case of the $LiPF_6$-based electrolyte solutions (see Fig. 5b). Similar to carbon oxidation, POF_3 generation would require oxygen from the EC molecules, but it is hard to find a reasonably feasible mechanism for this in the absence of an oxygen containing cathode active mass like layered transition metal oxides active-materials. However, here we used electrodes containing only carbon, that cannot release oxygen (indicated also by the absence of a chemical oxidation pathway for the electrolyte solutions with electrodes containing only carbon).[20] This raises the question whether the POF_3 we detect in our OEMS experiments is really generated in actual battery cells? As pointed out in our recent work on POF_3 and PF_5 quantification,[14] POF_3 signals detected in our OEMS setup (and likely also in other on-line mass spectrometer setups) can derive either from evolved POF_3 and/or from evolved PF_5,[14] as the latter is essentially quantitatively converted to POF_3 in the inlet system of our OEMS due to its reaction with oxygen-containing surface species at the stainless steel surfaces (either surface oxides or adsorbed water) in the low-pressure inlet tubing (at ca. 10^{-5} mbar; e.g., $PF_5 + H_2O \rightarrow POF_3 + 2HF$). The apparent "$POF_3$" signal starting already at ~4.0 V vs Li^+/Li (see Fig. 5b) is consistent with the data in our recent study[14] and corresponds to the formation of PF_5 in the cell (detected as "POF_3" by OEMS), caused by the electro-oxidation of ethylene glycol (EG) impurities at ~4.0 V vs Li^+/Li (Eq. 6) to the associated aldehyde and protons,[14,62] whereby the protons were shown to react rapidly with PF_6^- anions to PF_5 and HF (Eq. 7[14]):

$$C_2H_6O_2 \rightarrow C_2H_4O_2 + 2H^+ + 2e^- \quad [6]$$

$$PF_6^- + H^+ \leftrightarrow PF_5 + HF \quad [7]$$

Here it should be noted that EG impurities are generated from the hydrolysis of EC[63] with trace H_2O (Eq. 8; as well as Scheme 1 in Ref. 63):

$$C_3H_4O_3 + H_2O \rightarrow C_2H_6O_2 + CO_2 \quad [8]$$

At higher potentials (above ~4.8 V vs Li^+/Li at 25 °C and ~4.5 V vs Li^+/Li at 50 °C; see Fig. 4), protons can also be generated by the electro-oxidation of the ethylene carbonate solvent (see Scheme 1 in Ref. 61), which then allows for the continuous formation of PF_5 via Eq. 7. Reactions 6 and 7 have been proven unambiguously by adding small quantities of ethylene glycol (or ethanol) to carbonate electrolyte with $LiPF_6$ salt[62]: upon oxidation of the alcohol at ~4.0 V vs Li^+/Li, PF_5 was generated and subsequently detected as POF_3 in OEMS experiments.[62]

In summary, the electro-oxidation of ethylene glycol impurities (above ~4.0 V vs Li^+/Li) and EC (above ~4.5 V vs Li^+/Li at elevated temperatures) leads to protic decomposition products. Since we use our two-compartment cell[19,26] for this study, these species cannot travel to the anode side to get reduced. Accordingly, they remain in the catholyte compartment and the generated protons lead to HF generation with the PF_6^- anions producing PF_5 gas (see Eq. 7). Thereby, PF_5 is detected as "POF_3" in our OEMS system[14] (and probably in most other mass spectrometry based detection systems). The residual oxygen containing electrolyte decomposition products, e.g., $C_2H_3O^{\cdot}$,[14] then combine with the very reactive Lewis acid PF_5 to stable O-, F-, and P-containing surface species (see Figs. S6–S8), rather than providing oxygen for carbon oxidation. According to our EC oxidation mechanism,[14,17,61] this would also mean that the reaction intermediates could not further decompose and abstract CO, which is consistent with the fact that we do not detect CO formation in $LiPF_6$-based electrolyte solutions. For the LiTFSI and $LiBF_4$ based electrolyte solutions, the more than one order of magnitude lower OEMS signals even at 5.0 V vs Li^+/Li, compared to the response of the $LiPF_6$-based solutions (see Fig. 5), do not allow a more detailed analysis of the oxidation reactions.

The observed POF_3 signal (derived from $LiPF_6$ breakdown into PF_5 and HF via protons created at high anodic potentials) can be used for an order of magnitude estimation of $LiPF_6$ consumption. We observe ~1000 ppm POF_3 at 50 °C and 5.0 V vs Li^+/Li, which corresponds to ~0.5 μmol POF_3 in our cells (~10 ml internal volume). For every mole of POF_3 we detect, one mole of $LiPF_6$ has been converted via $PF_6^- + H^+ \leftrightarrow PF_5 + HF$. Thus, ~0.5 μmol $LiPF_6$ have been consumed in this oxidative pathway. The total amount of $LiPF_6$ in our cells is ~360 μmol, since we use 240 μl of 1.5 M $LiPF_6$ in EC. In summary, only ~0.1% of the $LiPF_6$ is consumed by oxidation pathways. If such a consumption rate would be sustained over a longer time period, there could be substantial salt loss. However, the POF_3 signal already starts to level off when most electrolyte solvent impurities are consumed by oxidation to protons (see Fig. 5b and our alcohol impurity estimations). Quantification and ultimately elimination of acidic species like POF_3 and PF_5, is highly important for long-lived lithium-ion cells, since these acidic species accelerate the thermal decomposition of lithium alkyl carbonates, the primary constituents of the anode SEI.[64–66]

Conclusions

We evaluated in this study the high-voltage stability of carbon (used as the conductive additive in composite cathodes) and EC solutions containing the lithium salts $LiClO_4$, $LiPF_6$, $LiBF_4$, and LiTFSI in a temperature range between 25 °C and 60 °C. We could differentiate between carbon and electrolyte solution oxidation by using fully ^{13}C labeled carbon electrodes and regular $^{12}C_3$ ethylene carbonate as the electrolyte solvent. $^xCO_2$ and ^xCO generation from the decomposition of carbon (x = 13) and electrolyte (x = 12) was quantified in situ by means of On-line Electrochemical Mass Spectrometry in sealed two-compartment cells.

Our main findings are that conductive carbon is stable with $LiPF_6$ solutions as opposed to solutions comprising $LiClO_4$ as the lithium salt. However, strong EC oxidation was observed at temperatures around 50 °C, and a considerable amounts of gaseous side products like HF and PF_5 are generated along with other oxidative decomposition products (e.g., surface species detected on the electrodes). LiTFSI is relatively stable, but provides no passivation for the aluminum foils used as the main cathodes' current collectors. The use of $LiBF_4$ as a lithium salt leads to a ~4-fold higher oxidative stability of the electrolyte solution, while the conductive carbon is equally stable as with $LiPF_6$. Judging only from its performance in high-voltage stability tests, $LiBF_4$ is therefore better suited than $LiPF_6$ for the cathode side in high-voltage lithium-ion cells.

Acknowledgments

The authors gratefully acknowledge BASF SE for financial support of this research through the framework of its Scientific Network on Electrochemistry and Batteries. We thank Dr. Yossi Gofer for his advice in designing the XPS experiments. Further, we thank Dr. Daniel Sharon, Dr. Daniel Hirschberg, and Dr. Sivan Okashi for their help with the experiments carried out in Israel.

ORCID

Michael Metzger https://orcid.org/0000-0002-5512-8541
Sophie Solchenbach https://orcid.org/0000-0001-6517-8094
Gregory Salitra https://orcid.org/0000-0003-4309-4249
Doron Aurbach https://orcid.org/0000-0001-8047-9020
Hubert A. Gasteiger https://orcid.org/0000-0001-8199-8703

References

1. G. E. Blomgren, *J. Electrochem. Soc.*, **164**, A5019 (2017).
2. G. M. Veith, J. Nanda, L. H. Delmau, and N. J. Dudney, *J. Phys. Chem. Lett.*, **3**, 1242 (2012).
3. H. Han, S. Zhou, D. Zhang, S. Feng, L. Li, and K. Liu, *J. Power Sources*, **196**, 3623 (2011).
4. E. R. Logan, D. S. Hall, M. M. E. Cormier, T. Taskovic, M. Bauer, I. Hamam, H. Hebecker, L. Molino, and J. R. Dahn, *J. Phys. Chem. C*, **124**, 12269 (2020).
5. E. R. Logan, E. M. Tonita, K. L. Gering, L. Ma, M. K. G. Bauer, J. Li, L. Y. Beaulieu, and J. R. Dahn, *J. Electrochem. Soc.*, **165**, A705 (2018).
6. Y. Zou, Y. Shen, Y. Wu, H. Xue, Y. Guo, G. Liu, L. Wang, and J. Ming, *Chem. - A Eur. J.*, **26**, 7930 (2020).
7. M. Nie and B. L. Lucht, *J. Electrochem. Soc.*, **161**, A1001 (2014).
8. M. Nie, D. Chalasani, D. P. Abraham, Y. Chen, A. Bose, and B. L. Lucht, *J. Phys. Chem. C*, **117**, 1257 (2013).
9. B. Markovsky, F. Amalraj, H. E. Gottlieb, Y. Gofer, S. K. Martha, and D. Aurbach, *J. Electrochem. Soc.*, **157**, A423 (2010).
10. B. Streipert, S. Röser, J. Kasnatscheew, P. Janßen, X. Cao, R. Wagner, I. Cekic-Laskovic, and M. Winter, *J. Electrochem. Soc.*, **164**, A1474 (2017).
11. R. Jung, M. Metzger, F. Maglia, C. Stinner, and H. A. Gasteiger, *J. Electrochem. Soc.*, **164**, A1361 (2017).
12. I. Buchberger, S. Seidlmayer, A. Pokharel, M. Piana, J. Hattendorff, P. Kudejova, R. Gilles, and H. A. Gasteiger, *J. Electrochem. Soc.*, **162**, A2737 (2015).
13. C. L. Campion, W. Li, and B. L. Lucht, *J. Electrochem. Soc.*, **152**, A2327 (2005).
14. S. Solchenbach, M. Metzger, M. Egawa, H. Beyer, and H. A. Gasteiger, *J. Electrochem. Soc.*, **165**, A3022 (2018).
15. J. Kim, G. Lee, H. Kim, J. Lee, H. Park, H. Ryu, and S. M. Oh, *J. Electrochem. Soc.*, **164**, 2418 (2017).
16. L. D. Ellis, I. G. Hill, K. L. Gering, and J. R. Dahn, *J. Electrochem. Soc.*, **164**, A2426 (2017).
17. M. Metzger, J. Sicklinger, D. Haering, C. Kavakli, C. Stinner, C. Marino, and H. A. Gasteiger, *J. Electrochem. Soc.*, **162**, A1227 (2015).
18. D. S. Strmcnik et al., "Electrocatalytic transformation of HF impurity to H2 and LiF in lithium-ion batteries." *Nat. Catal.*, **1**, 255 (2018).
19. M. Metzger, B. Strehle, S. Solchenbach, and H. A. Gasteiger, *J. Electrochem. Soc.*, **163**, A798 (2016).
20. R. Jung, M. Metzger, F. Maglia, C. Stinner, and H. A. Gasteiger, *J. Phys. Chem. Lett.*, **8**, 4820 (2017).
21. D. R. Gallus, R. Schmitz, R. Wagner, B. Hoffmann, S. Nowak, I. Cekic-Laskovic, R. W. Schmitz, and M. Winter, *Electrochim. Acta*, **134**, 393 (2014).
22. J. Wandt, A. Freiberg, R. Thomas, Y. Gorlin, A. Siebel, R. Jung, H. A. Gasteiger, and M. Tromp, *J. Mater. Chem. A*, **4**, 18300 (2016).
23. M. He, L. Boulet-Roblin, P. Borel, C. Tessier, P. Novák, C. Villevieille, and E. J. Berg, *J. Electrochem. Soc.*, **163**, A83 (2016).
24. A. Guéguen, D. Streich, M. He, M. Mendez, F. F. Chesneau, P. Novák, and E. J. Berg, *J. Electrochem. Soc.*, **163**, A1095 (2016).
25. A. Guéguen, C. Bolli, M. A. Mendez, and E. J. Berg, *ACS Appl. Energy Mater.*, **3**, 290 (2019).
26. M. Metzger, C. Marino, J. Sicklinger, D. Haering, and H. A. Gasteiger, *J. Electrochem. Soc.*, **162**, A1123 (2015).
27. J. C. Burns, A. Kassam, N. N. Sinha, L. E. Downie, L. Solnickova, B. M. Way, and J. R. Dahn, *J. Electrochem. Soc.*, **160**, A1451 (2013).

28. D. W. Abarbanel, K. J. Nelson, and J. R. Dahn, *J. Electrochem. Soc.*, **163**, A522 (2016).
29. D. Pritzl, A. Bumberger, M. Wetjen, J. Landesfeind, S. Solchenbach, and H. A. Gasteiger, *J. Electrochem. Soc.*, **166**, 582 (2019).
30. L. D. Ellis, J. Xia, A. J. Louli, and J. R. Dahn, *J. Electrochem. Soc.*, **163**, A1686 (2016).
31. C. Shen, D. Xiong, L. D. Ellis, K. L. Gering, L. Huang, and J. R. Dahn, *J. Electrochem. Soc.*, **164**, A3349 (2017).
32. N. Tsiouvaras, S. Meini, I. Buchberger, and H. A. Gasteiger, *J. Electrochem. Soc.*, **160**, A471 (2013).
33. D. NIST Mass Spec Data Center, S. E. Stein, https://webbook.nist.gov/cgi/cbook.cgi?Formula=CO2&NoIon=on&Units=SI&cMS=on; accessed 08/15/2020.
34. T. Mittermeier, A. Weiß, F. Hasché, and H. A. Gasteiger, *J. Electrochem. Soc.*, **165**, F1349 (2018).
35. R. Tang, K. Taguchi, H. Nishihara, T. Ishii, E. Morallón, D. Cazorla-Amorós, T. Asada, N. Kobayashi, Y. Muramatsu, and T. Kyotani, *J. Mater. Chem. A*, **7**, 7480 (2019).
36. K. Nomura, H. Nishihara, N. Kobayashi, T. Asada, and T. Kyotani, *Energy Environ. Sci.*, **12**, 1542 (2019).
37. D. Pritzl, S. Solchenbach, M. Wetjen, and H. A. Gasteiger, *J. Electrochem. Soc.*, **164**, A2625 (2017).
38. T. Mittermeier, A. Weiß, F. Hasche, G. Huebner, and H. A. Gasteiger, "PEM Fuel Cell Start-up/Shut-down Losses vs. Temperature for Non-Graphitized and Graphitized Cathode Carbon Supports." *J. Electrochem. Soc.*, **164**, F127 (2017).
39. M. Xu, L. Zhou, Y. Dong, Y. Chen, J. Demeaux, A. D. MacIntosh, A. Garsuch, and B. Lucht, *Energy Environ. Sci.*, **9**, 1308 (2016).
40. E. Cattaneo and J. Ruch, *J. Power Sources*, **44**, 341 (1993).
41. D. NIST Mass Spec Data Center, S. E. Stein, https://webbook.nist.gov/cgi/cbook.cgi?ID=C10049044&Mask=200#Mass-Spec accessed 08/15/2020.
42. D. NIST Mass Spec Data Center, S. E. Stein, https://webbook.nist.gov/cgi/cbook.cgi?ID=C13478201&Mask=200#Mass-Spec accessed 08/18/2020.
43. E. Cattaneo, B. Rasch, and W. Vielstich, *J. Appl. Electrochem.*, **21**, 885 (1991).
44. D. NIST Mass Spec Data Center, S. E. Stein, https://webbook.nist.gov/cgi/cbook.cgi?ID=C353504&Mask=200#Mass-Spec accessed 08/15/2020.
45. H. Yang, G. V. Zhuang, and P. N. Ross, *J. Power Sources*, **161**, 573 (2006).
46. D. NIST Mass Spec Data Center, S. E. Stein, https://webbook.nist.gov/cgi/cbook.cgi?ID=C75467&Mask=200#Mass-Spec accessed 08/15/2020.
47. T. Ma et al., *J. Phys. Chem. Lett.*, **8**, 1072 (2017).
48. D. NIST Mass Spec Data Center, S. E. Stein, https://webbook.nist.gov/cgi/cbook.cgi?ID=C75376&Units=SI&Mask=200#Mass-Spec accessed 08/15/2020.
49. X. Liang, Q. Pang, I. R. Kochetkov, M. S. Sempere, H. Huang, X. Sun, and L. F. Nazar, *Nat. Energy*, **6**, 17119 (2017).
50. S. Brutti and S. Panero, *Nanotechnol. Sustain. Energy*, **4**, 67 (2013).
51. A. Freiberg, M. Metzger, D. Haering, S. Bretzke, S. Puravankara, T. Nilges, C. Stinner, C. Marino, and H. A. Gasteiger, *J. Electrochem. Soc.*, **161**, A2255 (2014).
52. J. Xia, L. Ma, K. J. Nelson, M. Nie, Z. Lu, and J. R. Dahn, *J. Electrochem. Soc.*, **163**, A2399 (2016).
53. P. T. Yu, W. Gu, J. Zhang, R. Makharia, F. T. Wagner, and H. A. Gasteiger, "Carbon-Support Requirements for Highly Durable Fuel Cell Operation." *Polymer Electrolyte Fuel Cell Durability*, ed. F. N. Buchi, M. Inaba, and T. J. Schmidt (Springer, New York) (2009).
54. J. Wandt, A. T. S. Freiberg, A. Ogrodnik, and H. A. Gasteiger, *Mater. Today*, **21**, 825 (2018).
55. F. T. Wagner, B. Lakshmanan, and M. F. Mathias, *J. Phys. Chem. Lett.*, **1**, 2204 (2010).
56. R. P. Day, J. Xia, R. Petibon, J. Rucska, H. Wang, A. T. B. Wright, and J. R. Dahn, *J. Electrochem. Soc.*, **162**, A2577 (2015).
57. D. J. Xiong, L. D. Ellis, R. Petibon, T. Hynes, Q. Q. Liu, and J. R. Dahn, *J. Electrochem. Soc.*, **164**, A340 (2017).
58. D. J. Xiong, R. Petibon, M. Nie, L. Ma, J. Xia, and J. R. Dahn, *J. Electrochem. Soc.*, **163**, A546 (2016).
59. B. Strehle, S. Solchenbach, M. Metzger, K. U. Schwenke, and H. A. Gasteiger, *J. Electrochem. Soc.*, **164**, A2513 (2017).
60. T. Bond, J. Zhou, and J. Cutler, *J. Electrochem. Soc.*, **164**, A6158 (2017).
61. M. Metzger, B. Strehle, S. Solchenbach, and H. A. Gasteiger, *J. Electrochem. Soc.*, **163**, A798 (2016).
62. A. T. S. Freiberg, J. Sicklinger, S. Solchenbach, and H. A. Gasteiger, *Electrochim. Acta*, **346**, 136271 (2020).
63. M. Metzger, B. Strehle, S. Solchenbach, and H. A. Gasteiger, *J. Electrochem. Soc.*, **163**, A1219 (2016).
64. B. S. Parimalam, A. D. MacIntosh, R. Kadam, and B. L. Lucht, *J. Phys. Chem. C*, **121**, 22733 (2017).
65. S. K. Heiskanen, J. Kim, and B. L. Lucht, *Joule*, **3**, 2322 (2019).
66. S. K. Heiskanen, N. Laszczynski, and B. L. Lucht, *J. Electrochem. Soc.*, **167**, 100519 (2020).